# ResearchOnline@JCU



This is the author-created version of the following work:

Kamel, Michael S.A., Stoppiello, Craig Thomas, and Jacob, Mohan V. (2023) Single-step, catalyst-free, and green synthesis of graphene transparent electrode for organic photovoltaics. Carbon, 202 pp. 150-158.

Access to this file is available from:

https://researchonline.jcu.edu.au/78452/

© 2022 Elsevier Ltd. All rights reserved.

Please refer to the original source for the final version of this work:

https://doi.org/10.1016/j.carbon.2022.11.017

# Single-step, Catalyst-free, and Green Synthesis of Graphene Transparent Electrode for Organic Photovoltaics

Michael S. A. Kamel ab, Craig Thomas Stoppiello c and Mohan V. Jacob \*a

<sup>a</sup> Electronic Materials Research Lab, College of Science and Engineering, James Cook University,

Townsville 4811, Australia

<sup>b</sup> Physics Department, Faculty of Science, Minia University, P.O. Box 61519 Minia, Egypt

<sup>c</sup> Centre for Microscopy and Microanalysis, The University of Queensland, Australia.

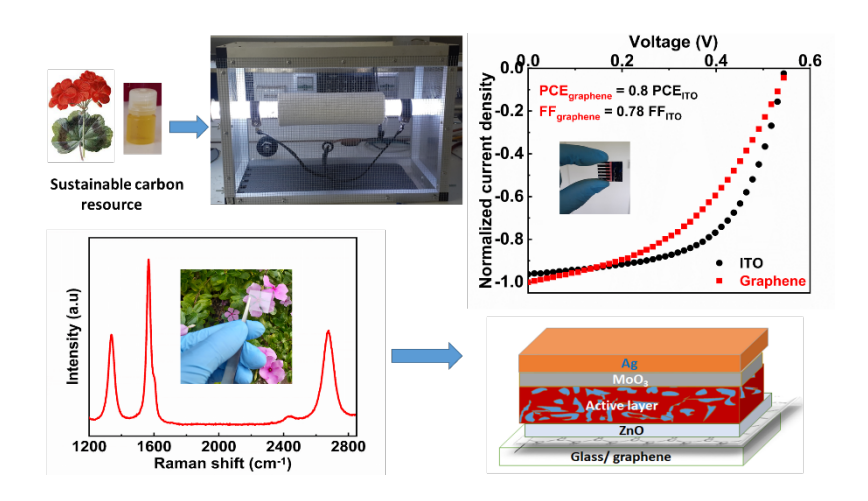
#### **Abstract**

Graphene is a promising transparent conducting electrode (TCE) for organic photovoltaics (OPVs) due to its outstanding optical and electrical properties. However, the high cost and complexity of graphene synthesis on transparent substrates as well as the use of hazardous carbon sources limits the large-scale application of graphene TCEs. This work reports a single-step synthesis of graphene TCEs on glass substrates for OPVs from plant extract by Radio frequency plasma enhanced chemical vapour deposition. This approach provides fast, cheap, and catalyst-free production of graphene from a sustainable and environmentally-friendly carbon resource. The as-prepared graphene films reveal high quality structure with promising optical and electrical properties. Inverted OPV devices built on the as-synthesized graphene TCEs exhibit 80% of the power conversion efficiency of their indium tin oxide counterparts, and higher short circuit current density and open circuit voltage.

### **Keywords**

Transparent conducting electrode, Transfer-free graphene, Sustainable carbon source, Organic photovoltaics, Short circuit current density.

# **Graphical abstract**



#### 1. Introduction

Transparent conductive electrode (TCE) is a fundamental constituent for OPVs which transmits the incident sunlight towards the photoactive layer and collects the photo-generated charge carriers. Indium tin oxide (ITO) is the most commonly-used TCE for OPVs and other optoelectronics due to its high optical transmission and low sheet resistance [1-3]. However, the high production cost, brittle nature, and the rarity of indium represent the main limitations of ITO as TCE for optoelectronics [4-7]. The production of ITO accounts for 30% of the overall fabrication cost of an OPV device [8-11]. In addition, 87% of the total energy needed for the roll-to-roll manufacturing of OPVs is consumed during ITO deposition by vacuum sputtering [12]. Therefore, intensive research has been conducted over the past few years to develop ITO-free OPVs [6, 13-17]. Various TCEs have been proposed to replace ITO such as conducting polymers [18], metal thin films [19, 20], and metal oxides [21]. Moreover, 1 dimensional and 2 dimensional materials such as metal nanowires (NWs) [22, 23], carbon nanotubes (CNTs) [24], and graphene [25] have emerged as excellent TCE candidates. Graphene possesses outstanding optical and electrical characteristics which make it a perfect choice to replace ITO [26-28]. Nonetheless, the high cost and complexity associated with the multi-step graphene synthesis limit its large-scale application as TCE.

Several methods have been used to produce graphene TCEs for OPVs including chemical vapor deposition (CVD) [29-32], electrochemical exfoliation [15], spin [33] and spray [34] coating, and hot pressing. More details on these methods can be found in the systematic review by Garg et al. [25]. Among the abovementioned methods, CVD is the most common technique used to produce graphene TCEs for OPVs due to the high quality of the resulting graphene films [25, 35-37]. CVD uses a gaseous carbon source, mainly methane and ethane, and a carrier gas such as H<sub>2</sub> to produce graphene nanosheets on catalyst substrates such as copper and nickel at temperatures reaching 1000 °C. The synthesized graphene films are then transferred, in a multi-step procedure, onto glass or flexible substrate for TCE applications. The transfer process can result in significant deterioration to the graphene properties [25]. For damage-free transfer of graphene, highly-complicated and time consuming procedures such as that based on poly (methyl methacrylate) (PMMA) should be used. This transfer approach is based on the spin coating of PMMA support layer on top of the graphene: metal substrate which adheres firmly to the graphene layer to facilitate the removal of the metal substrate without considerable damage to graphene morphology. On the other hand, this transfer method includes multiple steps which can last for few days [38-41].

CVD-based graphene TCEs have major limitations such as the high cost and the complexity of synthesis and/or transfer procedures. In addition, many environmental hazards are associated with the use of unsustainable carbon sources (e.g. methane and ethane). Plasma enhanced (PE) CVD enabled graphene synthesis at lower temperatures on various substrates including glass. For example, a few studies reported the direct synthesis of graphene TCEs on glass using RF-PECVD for dyesensitized solar cells [42] and on polyestersulfone (PES) substrate for flexible perovskite solar cells (PSCs) [43]. Moreover, Wei and co-researchers [44] prepared graphene films for PSCs on different glass substrates at temperatures (600-750 °C) using copper-foam-assisted PECVD approach. However, all of those approaches [42-44] were based on an environmentally-hazardous carbon source (methane), carrier gases and long reaction times of two to three hours. Moreover, in case of graphene synthesis on PES [43], a thin layer of titanium was deposited first on the PES substrate by DC sputtering at 150 °C in an Ar/H<sub>2</sub> atmosphere prior to the RF PECVD step which in its turn increases the overall cost and complexity of the procedure. The resulting graphene films in ref. [44] had high defect concentrations with I<sub>D</sub>/I<sub>G</sub> ratio in the range of 1.4 - 1.6. Consequently, an additional two-step procedure was followed to improve the characteristics of the as synthesized graphene films using

AgNWs and PH1000. Thus, more research is needed to address the aforementioned issues related to the existing approaches before large-scale commercialization of CVD-graphene TCEs for OPVs and other optoelectronics. Currently, there is need for direct synthesis of graphene TCEs for OPVs that can overcome the existing limitations.

In this manuscript, the feasibility of developing single-step synthesis of graphene TCEs for OPVs on commercial glass from an environmentally-friendly, cheap and sustainable resource of plant extract by RF PECVD is systematically studied. The reported approach enabled the rapid synthesis of large-area graphene films at 600 °C without a catalyst or carrier gas via a two-minute reaction. The asprepared films have shown uniform coating with low structural defects, high optical transmittance, and medium sheet resistance. Inverted geometry OPV devices based graphene electrodes were investigated and compared to ITO-based (reference) counterparts. The graphene-based OPVs have shown a promising performance with higher short circuit current density ( $J_{SC}$ ) and open circuit voltage ( $V_{OC}$ ) and realizing 80% and 78% of the power conversion efficiency (PCE) and fill factor (FF) of the reference device, respectively. Therefore, the obtained results confirm that reported approach is an excellent step-forward towards the large-scale, time- and cost-effective and sustainable production of graphene TCEs for OPVs and other optoelectronic devices.

# 2. Experimental Methods

#### 2.1. Fabrication of graphene electrodes

Graphene electrodes were prepared by RF PECVD method from pelargonium graveolens precursor (more details on the precursor can be found in Table S1 and Fig. S1 and S2, supporting information) on commercial glass substrates. Prior to fabrication, substrates were cleaned through successive ultra-sonication in DI water with detergent, DI water, acetone, and isopropyl alcohol for 10 minutes each. A custom-made RF PECVD reactor and a heater was used to synthesize graphene electrodes. A representative image to the RF PECVD used in the present research can be found in Fig. S3. The reactor is connected to a vacuum pump at one side while the other side is connected to the precursor inlet. The precursor vapor molecules reach the reaction zone under the influence of vacuum without the need to heat the precursor due to its volatility at room temperature. The desired RF power is applied to the reactor from CESAR 1312 RF power generator at a fixed frequency of 13.56 MHz through two copper rings (electrodes) via matching unit (Navio RF matching network – Advanced Energy -M/N 3155401-002 C). Graphene samples were prepared at various RF input powers (200, 300, and 500 W) at a temperature of 600 °C, a pressure of 5×10<sup>-2</sup> mbar and deposition time of two minutes.

# 2.2. Fabrication of OPV devices

Inverted architecture OPV devices were fabricated with the structure glass/graphene/ZnO/Active layer/MoO<sub>3</sub>/Ag. In this work, two different active layers based on P3HT: PC<sub>70</sub>BM and PM6: Y6 were employed. A control (reference) device with typical structure was fabricated on ITO-coated glass, for comparison. For graphene-based devices, a relatively thick silver layer was first deposited using thermal evaporation on top of one side of the substrate to resist the removal of ZnO sol-gel and P3HT: PC<sub>70</sub>BM after spin coating to define the cathode. For the reference OPV device, non-patterned ITO-coated glass substrates were utilized. The ITO substrate was immersed in a mixture of HCl: HNO3: deionized water (2: 1: 2 vol./vol.) for 10 minutes to generate the proper pattern on ITO substrates, with the help of sticky tape, to fit the custom-made deposition mask and test board which were used with graphene-based device to achieve a fair comparison between their photovoltaic performance. After that, ITO substrates were cleaned via four subsequent 10-minute sonication steps in DI water and decon 90, DI water, acetone, and isopropyl alcohol followed by air drying and then left overnight in drying oven at 90 °C to remove any residues. Prior to spin coating of ZnO sol-gel,

both graphene- and ITO-coated substrate were treated by air plasma under a pressure of 0.03 mbar at RF power of 3 W for 30 seconds to obtain uniform and continuous coating. ZnO sol-gel was synthesized according to the procedure reported elsewhere [45]. ZnO sol-gel was spin coated at 4000 rpm for 60 s, and then ethanol-wet cotton swabs were used to define the electrodes. After that, the coated substrate was thermally annealed on a hot plate at 170 °C for 30 minutes in air. For the deposition of the active layer, the substrates were moved into a nitrogen-filled glovebox. A 30 µl of P3HT: PC<sub>70</sub>BM (1: 0.8 wt/wt) with total concentration of 25 mg ml<sup>-1</sup> dissolved in Chlorobenzene was spin coated on top of ZnO layer at 2000 rpm to produce ~ 90 nm thick active layer. A 10-minute annealing was then conducted on a hotplate at 120 °C inside the glovebox. For PM6: Y6 active layer, a total concentration of 16 mh ml<sup>-1</sup> (D: A = 1: 1.2) dissolved in chloroform with 0.5% vol/vol 1chloronaphthalene solvent additive was used. PM6: Y6 solution was spin coated at 3000 rpm for 60 seconds withouth any post annealing. Finally, the substrates were transferred to HIND HIVAC 12A4D thermal evaporator using a custom-made shadow mask for the deposition of MoO3 (3.5 nm) and Ag (130 nm) top electrode. The deposition rate of MoO<sub>3</sub> was 0.2 Å s<sup>-1</sup> while for Ag anode an initial rate of 0.5 Å s<sup>-1</sup> was used for the first 20 nm, and then increased up to 1.9 Å s<sup>-1</sup>. The active area of 6 mm<sup>2</sup> for all devices was defined by the custom-made deposition mask. Descriptive images for the prepared graphene electrodes and graphene-based OPV devices are given in Fig. S4.

#### 2.3. Characterization of graphene films

The formation of graphene films was confirmed with Raman spectrometer (Rainshaw Raman Microscope, 514 nm laser). Scanning electron microscope (JEOL Field Emission SEM) and atomic force microscope (AFM) NT-MDT NTEGRA, Moscow, Russian) were used to investigate the morphology of graphene films. Structural features such as the number of layers and purity of the synthesized graphene samples were investigated using transmission electron microscope (TEM) (Hitachi HT7700 TEM equipped with LaB6 filament operating at 120 kV) and X-ray photoelectron spectroscopy (XPS) was performed using a Kratos AXIS SUPRA PLUS instrument with a monochromatic Al Kα x-ray source (hv = 1486.6 eV) operated at 10 mA emission current and 12 kV anode potential. Ellipsometer (J.A. Woollam Co. Inc. M-2000D) was used to study the optical transmittance of graphene films, while their sheet resistance (R<sub>s</sub>) was measured by fourpoint probe method using Keithley source measure unit (2636A) and a probe station (Everbeing int'l corp., C series starter probe station and EB-050 micropoisitioners) as shown in Fig. S5.

#### 2.4. Device characterization

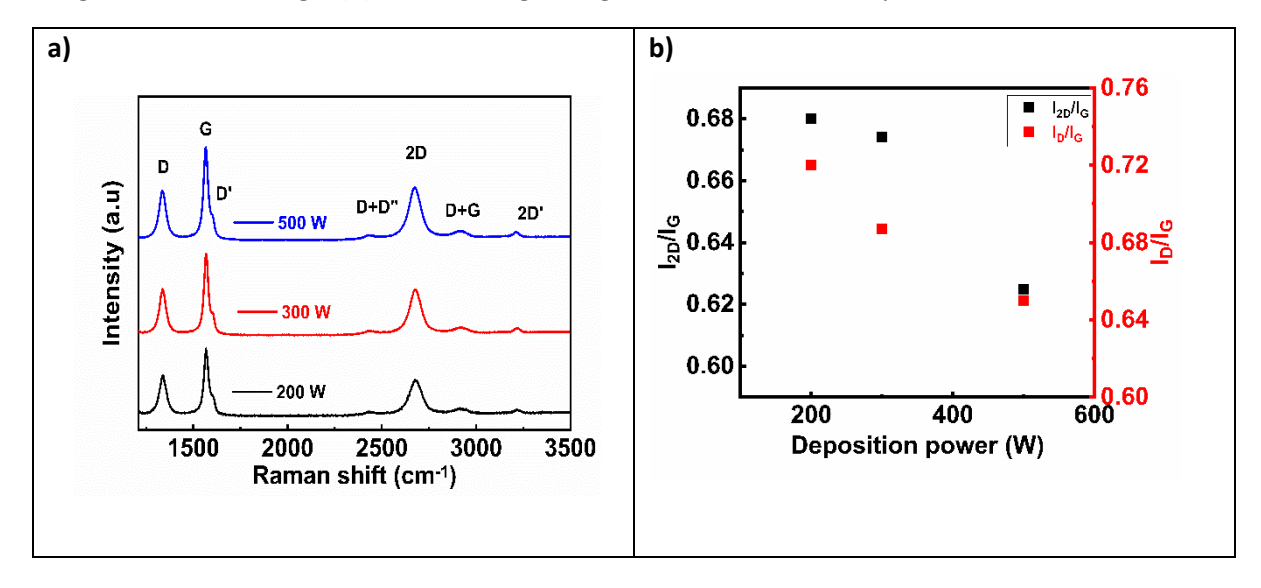
The performance of the fabricated devices was investigated via studying their current density-voltage (J-V) characteristic curves. J-V data were collected using Keithley Source meter unit (model 2636A) and an especially-designed test board under the illumination of AM1.5 G solar simulator (ABET Sunlite) with intensity of 100 mW cm<sup>-2</sup>. The optical intensity of the solar simulator was calibrated using a reference Si solar cell. All J-V measurements were carried out in air and directly after the deposition of the metal electrode. All devices were characterized without encapsulation.

#### 3. Results and discussion

The Raman spectra for graphene samples prepared on glass substrates at different deposition RF power levels (Fig. 1) confirm the successful formation of graphene on commercial glass substrates without any carrier gases. The investigated samples have quite similar spectra with relatively sharp 2D peaks and varying  $I_{2D}/I_G$  and  $I_D/I_G$  ratios with the deposition power. The G (~ 1567 cm-1) and 2D (~ 2673 cm-1) peaks represent the characteristic in-plane E2g vibration of sp2 hybridized carbon and the second order of the zone-boundary phonons, respectively. The 2D peak has been identified as an evidence on the formation of the graphene-like structure [46]. The D peak at ~ 1336 cm<sup>-1</sup> accounts for the structural defects within graphene lattice such as wrinkles, vacancies, dislocations, edges, etc.

Furthermore, other peaks related to structural defects such as peak D' which arises as a shoulder at the G-peak around 1610 cm<sup>-1</sup>, D+D" ( $^{\sim}$  2426 cm-1), D+G ( $^{\sim}$  2917 cm<sup>-1</sup>), and 2D' (3211 cm<sup>-1</sup>) appeared with almost negligible intensities. The ratio of the  $I_D/I_G$  for the synthesized graphene samples on glass substrates ranged from 0.72 to 0.65 which is less than other graphene films prepared by the same method using  $H_2$  carrier gas and at higher temperatures (>700  $^{\circ}$ C) on different substrates [47].

The ratio of  $I_D/I_G$  and  $I_{2D}/I_G$  decreased with increasing the deposition power from 200 to 500 W (Fig. 1(b)) The ratio of I<sub>2D</sub>/I<sub>G</sub> decreases with increasing the number of graphene layers. By increasing the deposition power, the number of layers increased which reflected on the TEM images, sheet resistance and optical transmission of the investigated films as will be discussed in later sections. The increased number of graphene layers at high power can be attributed to the high growth rate of graphene as a result of the increased decomposition of the precursor molecules induced by the high energy of the plasma species. The ratio of I<sub>D</sub>/I<sub>G</sub> represents the defects in graphene films and increases with the presence of more defects. The  $I_D/I_G$  ratio for the investigated samples was found to decrease at high RF deposition power which may be attributed to the purity of graphene films and the presence any impurity atoms within the lattice (as confirmed by XPS data, to be discussed later). Structural defects greatly influence the electrical properties of graphene as will be discussed in sheet resistance section. In order to have a deeper insight on the structure of the investigated graphene films, transmission electron microscope (TEM) was used. Fig. 1(c-h) shows TEM images for the assynthesized graphene samples, which shows multi-layers of graphene which is in agreement with Raman data. The number of graphene layers was found to increase with the deposition RF power as shown in Fig. 1 (C, f, and g) which confirms the behavior of I<sub>2D</sub>/<sub>IG</sub> ratio [48] in Fig. 1(b). The variation in the number of graphene layers explains the improved electrical conductivity and the reduced optical transmission for graphene films synthesized at higher power as will be discussed later in this work. The interlayer spacing within the investigated graphene films was found to be 0.33 nm as shown in Fig. 1(d) which greatly matches literature and the theoretical value of 0.33 nm [44, 49, 50]. Moreover, the high resolution TEM images reveal the highly ordered carbon atoms within graphene lattice as shown in case of sample prepared at 300 W in Fig. 1(e). On the other hand, the presence of structural defects such as voids or vacancies within graphene lattice can be observed from TEM images, as shown in Fig. 2(h), which is in good agreement with Raman spectra.



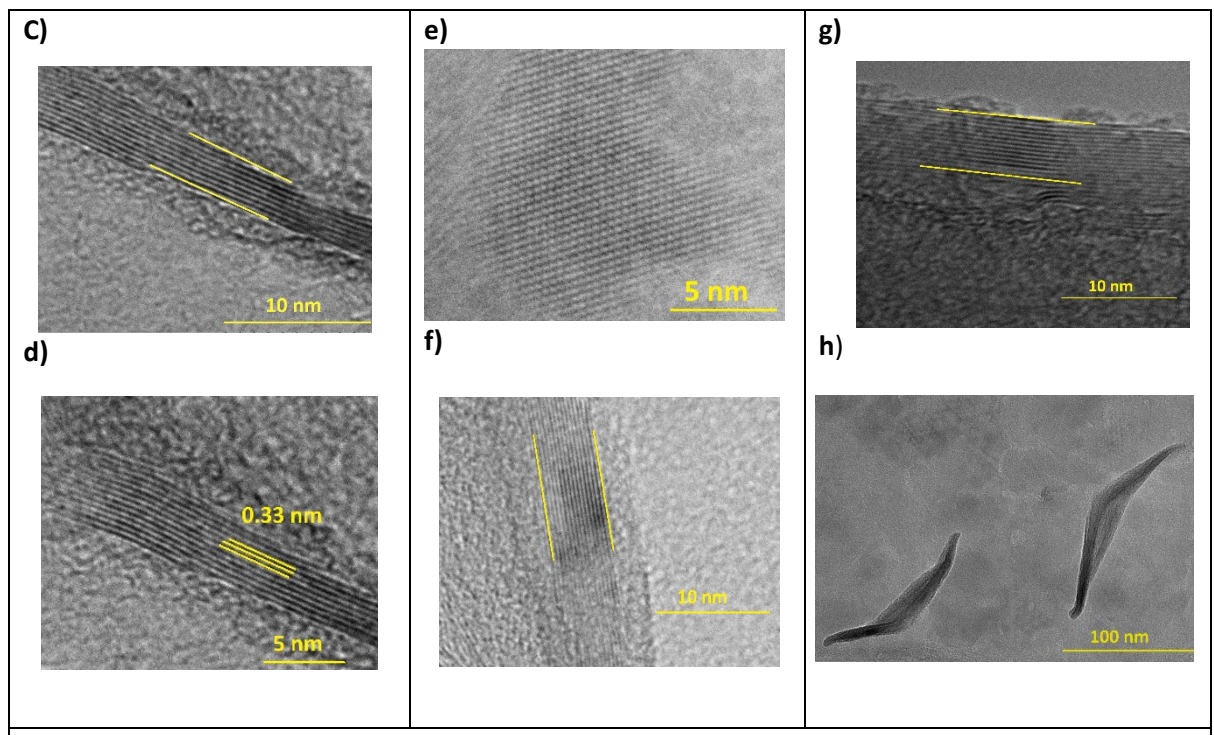


Fig. 1. (a) Raman spectra for graphene samples prepared at various RF input power levels. (b) The variation of  $I_D/I_G$  and  $I_{2D}/I_G$  of graphene films with RF deposition power. (c-e) Representative TEM images for graphene samples synthesized at 200 W (c and d), 300 W (e and f), and 500 W (g and h).

To better understand the chemical bonding within the synthesized graphene films, they were investigated by x-ray photoelectron spectroscopy (XPS). Fig. 3 shows the survey scan and high resolution XPS spectra for the graphene films prepared at 200 W, 300 W and 500 W. It can be observed from the XPS spectra that carbon represents the major constituent of the investigated film with a minor amount of oxygen, as summarized in Table 1, which indicates the high quality of the synthesized graphene films. The presence of the O 1s peak at 531 eV can be attributed to oxygen-rich components within the precursor molecules as well as the exposure of graphene films to the ambient atmosphere [47, 51]. The minor peaks at binding energies (B.E.) of 105 eV and 1071 eV) represent the Si 2p and Na 1s, respectively, which can be attributed to the glass substrate surface CasaXPS software was used for the deconvolution of the C 1s peak which resulted in a major peak at 284.52 eV due to the sp<sup>2</sup> hybridized hexagonal graphene lattice [52, 53]. Other peaks with lower contribution to the overall fitting area were also observed at 283.74 eV and 288.49 eV which correspond to C-O and C=O, respectively. The emergence of C-O and C=O can be ascribed to the exposure of the investigated samples to ambient oxygen which reacts with the active sites within graphene films such as defects and edges [52, 54]. Furthermore, two peaks were observed at 294.52 and 291.09 eV which assign for the Plasmon loss features (PL 1 and PL 2) associated with graphitic carbon [54]. It can also be observed that carbon content within the investigated films increased from (86.82%) to 96.83% with a simultaneous drop in the oxygen percentage to < 2% with increasing the deposition RF power from 200 W to 500 W which may be assigned to the glass background (substrate) effect due to the surface sensitive nature of the technique. Typically, only the top 5-10 nm layer of a sample is accessible using XPS; [55] Raman, TEM and optical transmission results indicate that the sample at 200 W has the fewest number of graphene layers.

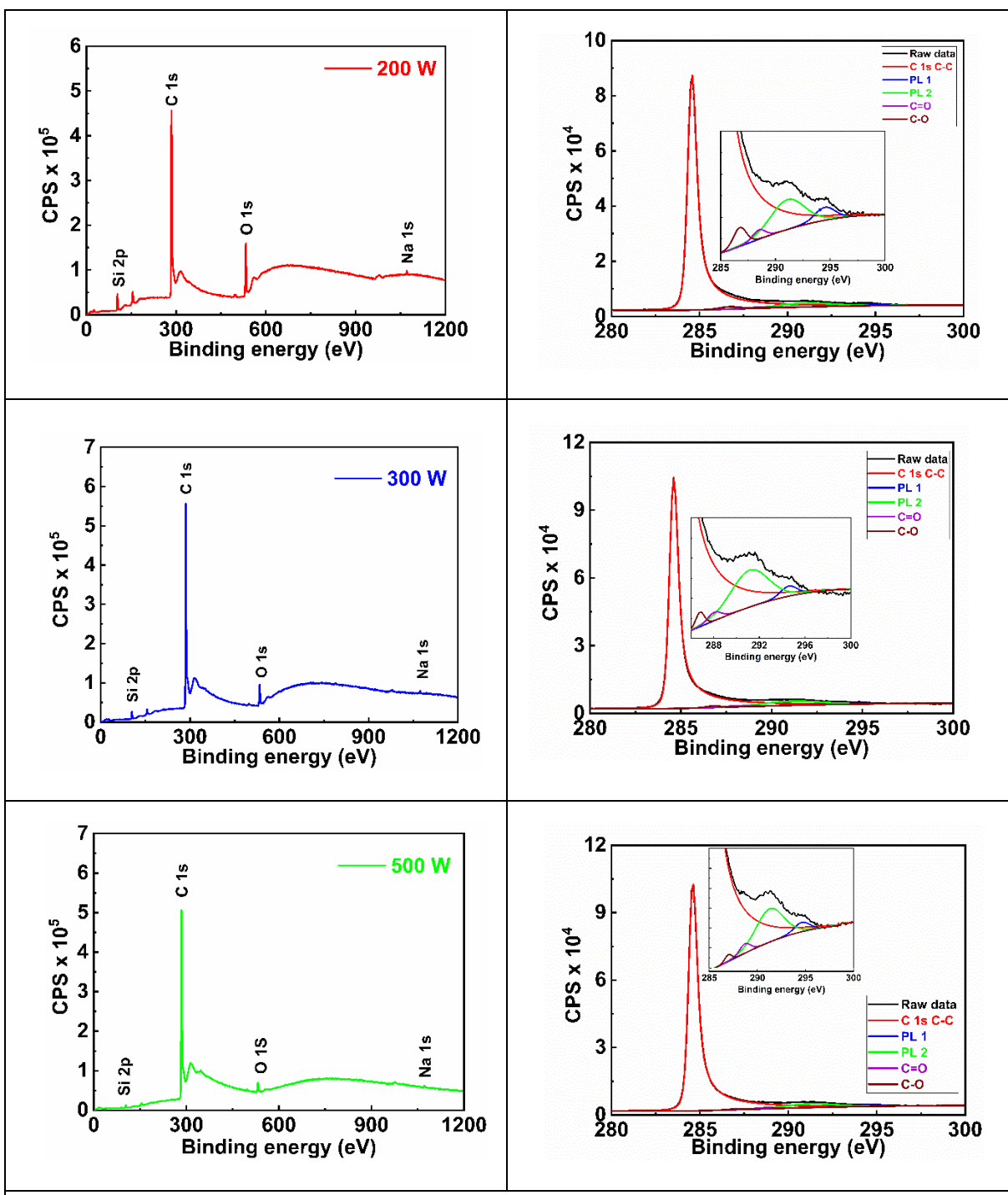


Fig. 2. XPS survey scans (left hand panel) of the graphene samples prepared at 200 W (top), 300 W (middle) and 500 W (bottom) alongside the corresponding C 1s high resolution (HR) scan for each sample. The survey scans show that the surfaces of the samples primarily consist of carbon and oxygen, with smaller Si and Na peaks attributed to the sample support. The C 1s HR regions follow an asymmetric pattern associated with graphitic carbon. Various C-O bonds and plasmon loss features are shown inset.

Table 1

Elemental surface compositions of graphene samples prepared at various RF input power.

| RF power (W) | Na 1s (%) | O 1s (%) | C 1s (%) | Si 2p (%) |
|--------------|-----------|----------|----------|-----------|
| 200          | 0.30      | 8.06     | 86.82    | 4.82      |
| 300          | 0.18      | 3.65     | 93.91    | 2.27      |
| 500          | 0.13      | 2.06     | 96.83    | 0.98      |

The surface features of the synthesized graphene films was studied by SEM and AFM. The SEM images (Fig. 3) show quite uniform film with the presence of small vertically-oriented graphene nano-islands. It can be observed from Fig. 3(c) that the number of the graphene nano-islands is higher for the sample synthesized at 500 W. However, these islands do not form continuous interpenetrating networks. The morphology of graphene films synthesized by RF PECVD are greatly affected by the deposition parameters such as time, temperature, power, and substrate type and the utilization of carrier gas. For example, Jacob et al. [56] reported the formation of folded vertical graphene nano-sheets in continuous interpenetrating networks on Silicon and fused substrates at 800 °C and 500 W in the presence of H<sub>2</sub> carrier gas even at deposition time of 1 sec. The morphology of graphene films plays a crucial role in deciding their applications. Therefore, the synthesis parameters should be optimized to produce the desirable film morphology for a specific application. For optoelectronics, a TCE with smooth surface is more preferred to obtain uniform coating of the other layers of the device and to reduce carrier recombination as will be discussed in the device performance section in the present research. The surface properties of the investigated graphene films were confirmed by AFM (Fig. S6). The root mean square (rms) roughness of the as-synthesized graphene films on glass substrates was found to increase with increasing input RF power. The samples prepared at 200 and 300 W revealed guite similar features with relatively low rms surface roughness of 2.59 and 3.9 nm, while the sample synthesized at 500 W exhibited much higher rms roughness of 8.52 nm. The high surface roughness can be attributed to the vertical growth of the graphene nanosheets which increased at higher power as discussed above.

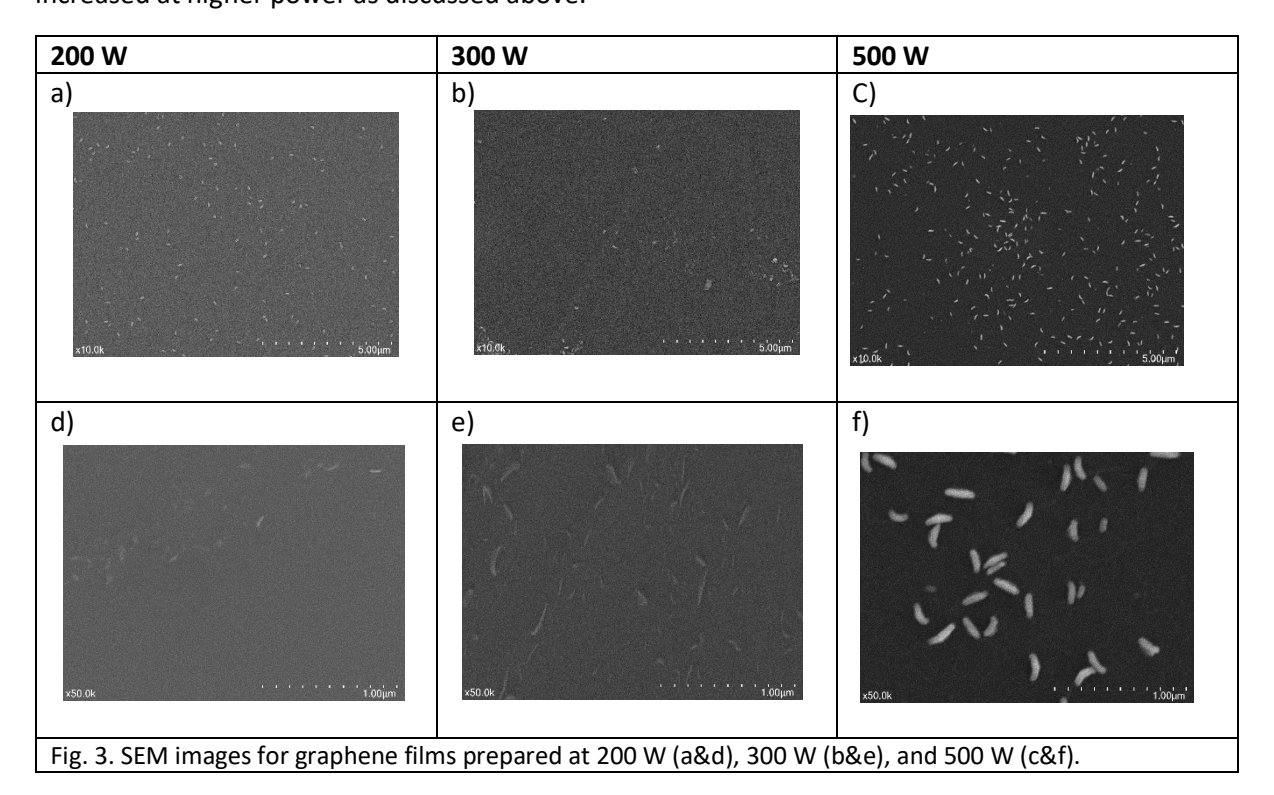


Fig. 4(a,b) shows the variation of the sheet resistance ( $R_s$ ) of graphene films with the RF deposition power. The values of  $R_s$  were extracted from the slope of the current-voltage (I-V) relation obtained via the four-point probe measurements. A square sample with a dimension of 12 mm was used for this measurement, where a fixed current was applied to the sided probes, while the voltage was measured across the internal probes. The value of Rs was calculated according to the equation below [57, 58]:

$$R_s = 4.53 \times C \frac{dV}{dI} \tag{1}$$

where,  $\frac{dV}{dI}$  is the slope of the straight line I-V relation (Fig. 4(a)) and C is a correction factor that depends on sample dimensions and the distance between the measurement probes. The sheet resistance is an important parameter for TCE materials for OPVs which affects the series resistance and the photovoltaic performance of the device. The lower the sheet resistance, the more efficient the TCE is. The high conductivity of the transparent electrode material improves the collection of the photogenerated charge carriers. It is clear from Fig. 4(b) that Rs decreases significantly with increasing the deposition RF power. Rs dropped from 1.6 K $\Omega/\Box$  to 0.97 K $\Omega/\Box$  when the applied plasma power increased from 200 to 500 W. This improvement in electrical properties can be attributed to the increase in the number of layers in graphene films as confirmed by Raman and TEM results. This drop in Rs is accompanied by a reduction in the film transparency which may cause a decrease in the PCE of the OPV device. The growth rate of graphene increases at high deposition power due to the enhanced decomposition rate of the precursor molecules by the highly energetic plasma species [47]. In addition, the electrical conductivity of graphene strongly depends on the presence of structural defects such as wrinkles, voids, dislocations, etc. The sheet resistance increases with increasing the defects in graphene films [59] which is in a great agreement with the findings in the present work. From Raman data (Fig. 1(b)), the ratio of I<sub>D</sub>/I<sub>G</sub> decreases with increasing the RF deposition power which shows less structural defects at high power and therefore the sheet resistance dropped. The effectiveness of a TCE material depends strongly on its optical transmission. An efficient TE should allow as much incident solar light as possible to reach the photoactive layer to generate the maximum photocurrent. The optical transmission of the synthesized graphene samples on glass substrates was investigated and compared to ITO. Fig. 4(c) displays the optical transmission of the investigated samples for wavelength range between 300 and 1000 nm. The graphene film prepared at 200 W had the highest transmission of 81% at 550 nm, while samples synthesized at 300 W and 500 W were less transparent with transmission of 67% and 65%, respectively. The sample prepared at 500 W exhibited lower transmission especially at shorter wavelengths due to the graphene nano-islands as confirmed by SEM images. It can be noticed that graphene (at 200 W) is more transparent to the wavelengths below 550 nm than ITO. Moreover, the transmission of graphene films prepared at higher power levels were also comparable to ITO at short wavelengths (< 550 nm). It is worthy to mention that, the optical transmission of an efficient TCE for OPVs should be matching with the absorption band of the active layer of the device. For example, for wide bandgap donor polymer, a TCE material with high transmission to the short wavelengths is preferred and vice versa in case narrow bandgap donors. The reduction in optical transmission of graphene samples at higher RF power is attributed to the increased number of layers and the formation of graphene nano islands. Therefore, a trade-off between optical and electrical properties of the TCE should be realized for the optimum device performance.

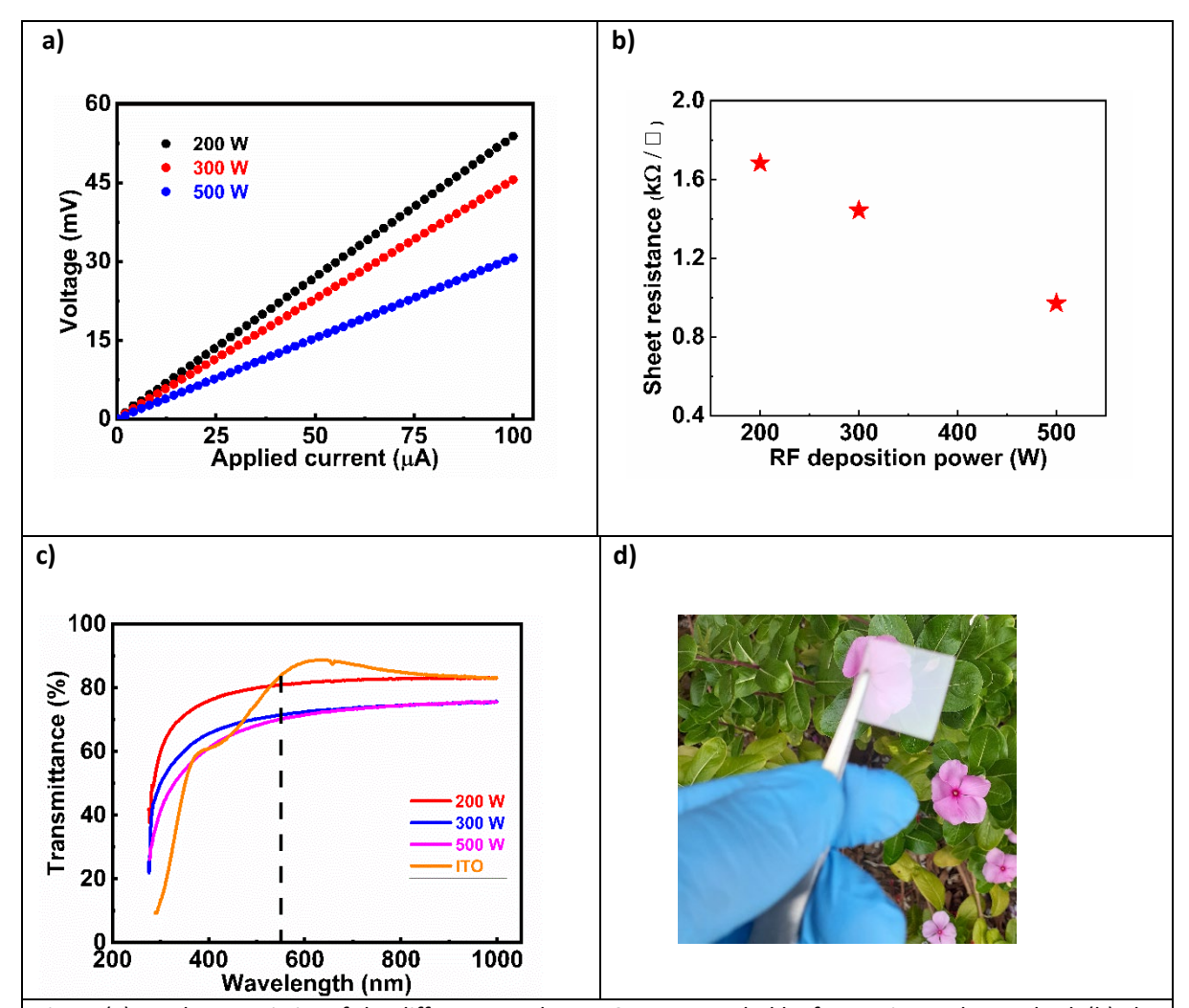


Fig. 4. (a) I-V characteristics of the different graphene TCEs as recorded by four-point probe method. (b) The variation of the sheet resistance of the synthesized graphene TCEs with RF input power. (c) Optical transmittance of the different graphene electrodes measured by J. Woollam Ellipsometer. (d) Typical image to the synthesized graphene TCE.

Fig. 5(a) shows the J-V characteristics of the graphene-based as well as the reference (ITO-based) OPV devices. The measured photovoltaic parameters of the devices are listed in Table 2. The  $J_{SC}$  and  $V_{OC}$  of the device built on graphene TCE prepared at 200 W RF input power are 5.17 mA/cm² and 0.56 V respectively, and the corresponding values of the ITO-counterparts are -4.95 mA/cm² and 0.55 V. The increase in  $J_{SC}$  in case of graphene-based device can be attributed to the high optical transmittance of graphene electrodes at short wavelengths (400 nm to 550 nm) compared to ITO (Fig. 4(c)). This wavelengths region (400 – 550 nm) represents the majority of the absorption range of the P3HT:PC<sub>70</sub>BM active blend [60]. It is worth mentioning that, the generation of photoelectrons in the photoactive layer of the device can also happen within the acceptor phase in addition to the electron donor material [61]. The PC<sub>70</sub>BM acceptor absorbs mainly at wavelengths between 380-500 nm [62]. Therefore, the OPV device with graphene electrode had higher  $J_{SC}$  than that based on ITO. Despite the higher  $J_{SC}$  and  $V_{OC}$  of the graphene-based device, its PCE was less than that of the ITO counterpart as a result of the reduced fill factor. The PCE and FF of the graphene-based device were found to be 1.14% and 0.39 which are equivalent to 72% and 67%, respectively, of those by the control device (1.58% and 0.58). The reduced FF of the graphene-based device can be attributed to the high sheet

resistance of graphene electrodes compared to ITO. The high sheet resistance of the TCE increases the series resistance of the device which leads to a drop in its fill factor as a result of carrier recombination [63]. In addition, graphene exhibited higher surface roughness than ITO as confirmed by AFM data which could be an additional recombination pathway resulting in FF drop. The relatively high sheet resistance of the synthesized graphene films can be attributed to the presence of structural defects such as wrinkles and voids as discussed above. For the devices fabricated on graphene electrodes synthesized at 300 and 500 W, their photovoltaic performance was close to that with graphene at 200 W. Their photovoltaic parameters are listed in Table 2. The  $J_{sc}$  increased slightly for both devices compared to the device based on graphene electrode prepared at 200 W although they exhibited lower optical transmission. The enhancement in  $J_{SC}$  for both devices can be attributed to the decrease in the sheet resistance of their graphene electrodes. Moreover, the drop in  $V_{OC}$  for the device based on graphene at 500 W may be attributed to the high surface roughness of the transparent electrode which impacts the uniformity of the spin coated ZnO electron transport layer and consequently the carrier recombination increases.

For further investigation to thethe feasibility of the synthesized graphene electrodes for OPVs, more devices based on the state-of-art active layer consisting of PM6: Y6 (donor: acceptor) were also fabricated (Fig. 5c). The device prepared on graphene TCE achieved a PCE of 4.94% while the unpatterned ITO-based counterpart exhibited 7.86%. In addition, the Jsc of the graphene-based device was higher than that of the reference device, but the V<sub>OC</sub> and FF were lower as listed in Table 2. These results are in a good agreement with the data for the devices based on P3HT: PC<sub>70</sub>BM active layer (Fig. 5a). It should be mentioned here that higher PCEs, between 12% to >15%, for PM6: Y6 based OPVs on ITO can be found in literature [64-66]. In order to validate the fabrication procedure used with our devices and figure out the possible reasons for their low PCEs compared to literature, more devices were fabricated based on pre-patterned ITO electrodes with similar sheet resistance and optical transmittance to the unpatterned ITO used for comparison with the investigated graphene electrodes. Higher PCEs reaching 12.2% were obtained for the devices built on pre-patterned ITO as shown in Fig. S7 in supplementary information which affirms the validity of the fabrication procedure of our devices. However, the variation of the PCE between pre-patterned and unpatterned ITO-based OPVs could be attributed to the different testboards used for the J-V measurements in both cases. Also, in case of OPVs built on unpatterned ITO and graphene TCEs, the contact of the testboard electrodes is through the thin Ag layers which can easily be damaged (Inset Fig. 5 a and c) in contrast to the pre-patterned ITO where the contact is achieved with the strongly adhered ITO strips (inset Fig. S7). Moreover, the deposition of the top electrode as well as J-V measurements for all devices in the present work was performed outside the glovebox which will contribute to the rapid degradation of the devices. The fast drop in the device performance is also displayed in Fig. S7 and Table S2.

The photovoltaic performance of an OPV device depends strongly on the structural, electrical and optical properties of the graphene TCE. Therefore, further enhancement in the performance of graphene-based OPVs, reported in the present work, can be realized by improving graphene characteristics, particularly the electrical conductivity and morphology [59]. In this regard, the device performance was enhanced through increasing the thickness of ZnO electron transport layer (ETL) on top of graphene electrodes. For instance, a double-layer ZnO was deposited on top of the graphene TCE (prepared at 300 W) via sequential spin coating at 3000 rpm and post annealing at 150 oC for 10 minutes [67]. The double-layer ZnO (D-ZnO) improved the FF of the device from 0.34 to 0.45 leading the PCE to increase from 1.06% to 1.27% (Fig. 6d and table 2). The increased FF and PCE can be attributed to the suppressed carrier recombination as a result of the improved morphology of the graphene which achieved a better interface with the active layer. We are conducting a continuing

research to achieve the best device performance to make the prepared graphene TCEs more comparable to ITO.

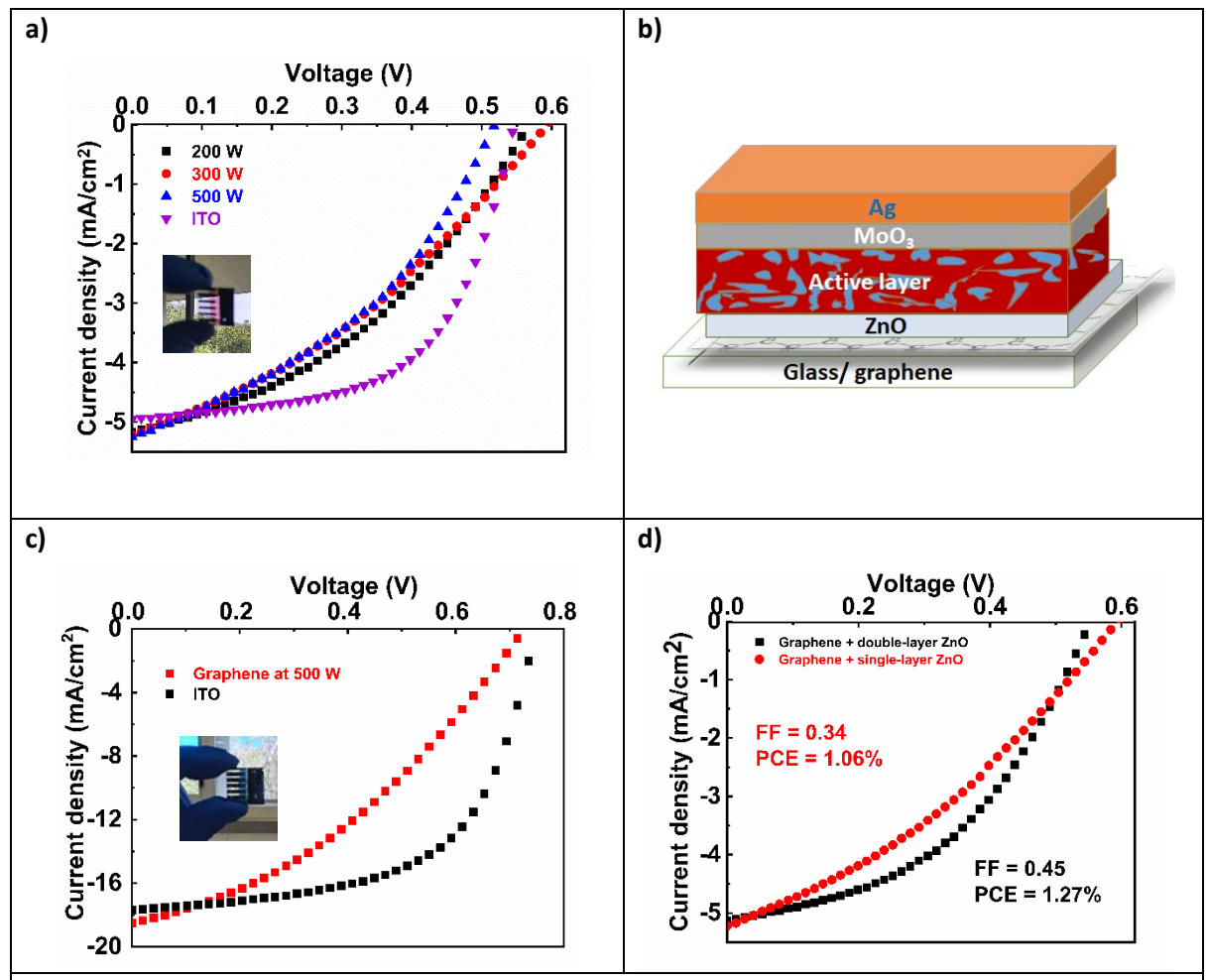


Fig. 5. (a) J-V characteristics of the inverted P3HT:  $PC_{70}BM$  OPV devices based on different graphene TCEs and ITO (reference device). (b) Schematic diagram to the structure of inverted OPV device employed in the present work. (c) J-V characteristics for PM6: Y6-based OPVs on graphene (500 W) and unpatterned ITO. (d) J-V characteristics for P3HT:  $PC_{70}BM$  devices based on graphene TCEs (at 300 W) with single- and double-layer ZnO ETL.

Table 2

The photovoltaic parameters of the OPV devices prepared on graphene and unpatterned ITO electrodes with different active layers.

| TCE              | Active layer              | J <sub>sc</sub> (mA/cm <sup>2</sup> ) | V <sub>oc</sub> (V) | FF   | PCE (%) |
|------------------|---------------------------|---------------------------------------|---------------------|------|---------|
| Graphene (200 W) |                           | -5.14                                 | 0.56                | 0.39 | 1.14    |
| Graphene (300 W) |                           | -5.22                                 | 0.59                | 0.34 | 1.06    |
| Graphene (500 W) | P3HT: PC <sub>70</sub> BM | -5.25                                 | 0.53                | 0.37 | 1.04    |
| Unpatterned ITO  |                           | -4.95                                 | 0.55                | 0.58 | 1.58    |
| Graphene (500 W) | PM6: Y6                   | -18.52                                | 0.72                | 0.37 | 4.94    |
| Unpatterned ITO  |                           | -17.69                                | 0.75                | 0.59 | 7.86    |
| Graphene (300 W) | P3HT: PC <sub>70</sub> BM | -5.14                                 | 0.56                | 0.45 | 1.27    |
| with Double-ZnO  |                           |                                       |                     |      |         |

#### 3. Conclusion

A low cost, rapid and direct synthesis of graphene TCEs on glass substrates for OPVs was presented. The reported approach uses an environmentally friendly and sustainable precursor without the need of a catalyst or a carrier gas. The synthesized graphene films showed remarkable structural, optical, and electrical features with a strong dependence on the RF deposition power. Optical transmittance between 81% - 65% at 550 nm at corresponding sheet resistances of 1.6 - 0.97  $K\Omega/\Box$  were recorded for the as-prepared graphene films. The OPVs built on the graphene TCEs had higher  $J_{SC}$  and  $V_{OC}$  and realized 80% of the PCE of the ITO-based device. Thus, the present study is a step-forward towards the large-scale commercialization of graphene electrodes for organic photovoltaics and other optoelectronic devices.

# **Supporting information**

# Acknowledgement

Michael S. A. Kamel would like to acknowledge the financial support by the college of Science and Engineering, James Cook University (JCU), Townsville, Australia through JCUPRS scholarship. We acknowledge and thank Dr Olexandra Marenych, CMM UQ for the TEM data acquisition.

#### **Conflicts of interest**

The authors declare no conflict of interest.

# **Data Availability Statement**

The data that support the findings of this study are available from the corresponding author upon reasonable request.

## References

- [1] Rahman MA, Rahim A, Maniruzzaman M, Yang K, Lee C, Nam H, et al. ITO-free low-cost organic solar cells with highly conductive poly (3, 4 ethylenedioxythiophene): p-toluene sulfonate anodes. Solar Energy Materials and Solar Cells. 2011;95:3573-8.
- [2] Du J, Zhang D, Wang X, Jin H, Zhang W, Tong B, et al. Extremely efficient flexible organic solar cells with a graphene transparent anode: Dependence on number of layers and doping of graphene. Carbon. 2021;171:350-8.
- [3] Cui H, Song W, Fanady B, Peng R, Zhang J, Huang J, et al. Flexible ITO-free organic solar cells over 10% by employing drop-coated conductive PEDOT: PSS transparent anodes. Science China Chemistry. 2019;62:500-5.
- [4] Kang JH, Choi S, Park YJ, Park JS, Cho NS, Cho S, et al. Cu/graphene hybrid transparent conducting electrodes for organic photovoltaic devices. Carbon. 2021;171:341-9.
- [5] Cho C-K, Hwang W-J, Eun K, Choa S-H, Na S-I, Kim H-K. Mechanical flexibility of transparent PEDOT: PSS electrodes prepared by gravure printing for flexible organic solar cells. Solar Energy Materials and Solar Cells. 2011;95:3269-75.
- [6] Wu J, Que X, Hu Q, Luo D, Liu T, Liu F, et al. Multi-length scaled silver nanowire grid for application in efficient organic solar cells. Advanced Functional Materials. 2016;26:4822-8.
- [7] Zhang J, Hu X, Li H, Ji K, Li B, Liu X, et al. High-Performance ITO-Free Perovskite Solar Cells Enabled by Single-Walled Carbon Nanotube Films. Advanced Functional Materials. 2021;31:2104396.
- [8] Manzano-Ramírez A, López-Naranjo EJ, Soboyejo W, Meas-Vong Y, Vilquin B. A review on the efficiency of graphene-based BHJ organic solar cells. Journal of Nanomaterials. 2015;2015.
- [9] Wang Y, Tong SW, Xu XF, Özyilmaz B, Loh KP. Interface engineering of layer-by-layer stacked graphene anodes for high-performance organic solar cells. Advanced materials. 2011;23:1514-8.

- [10] Wu J, Becerril HA, Bao Z, Liu Z, Chen Y, Peumans P. Organic solar cells with solution-processed graphene transparent electrodes. Applied physics letters. 2008;92:237.
- [11] Yin Z, Sun S, Salim T, Wu S, Huang X, He Q, et al. Organic photovoltaic devices using highly flexible reduced graphene oxide films as transparent electrodes. ACS nano. 2010;4:5263-8.
- [12] Krebs FC, Jørgensen M, Norrman K, Hagemann O, Alstrup J, Nielsen TD, et al. A complete process for production of flexible large area polymer solar cells entirely using screen printing—first public demonstration. Solar Energy Materials and Solar Cells. 2009;93:422-41.
- [13] Zheng X, Zuo L, Zhao F, Li Y, Chen T, Shan S, et al. High-Efficiency ITO-Free Organic Photovoltaics with Superior Flexibility and Up-Scalability. Advanced Materials. 2022:2200044.
- [14] Worfolk BJ, Andrews SC, Park S, Reinspach J, Liu N, Toney MF, et al. Ultrahigh electrical conductivity in solution-sheared polymeric transparent films. Proceedings of the National Academy of Sciences. 2015;112:14138-43.
- [15] Ricciardulli AG, Yang S, Wetzelaer GJA, Feng X, Blom PW. Hybrid silver nanowire and graphene-based solution-processed transparent electrode for organic optoelectronics. Advanced Functional Materials. 2018;28:1706010.
- [16] Chen X, Xu G, Zeng G, Gu H, Chen H, Xu H, et al. Realizing ultrahigh mechanical flexibility and> 15% efficiency of flexible organic solar cells via a "welding" flexible transparent electrode. Advanced Materials. 2020;32:1908478.
- [17] Huang J, Ren Z, Zhang Y, Liu K, Zhang H, Tang H, et al. Stretchable ITO-Free Organic Solar Cells with Intrinsic Anti-Reflection Substrate for High-Efficiency Outdoor and Indoor Energy Harvesting. Advanced Functional Materials. 2021;31:2010172.
- [18] Wan J, Xia Y, Fang J, Zhang Z, Xu B, Jinzhao W, et al. Solution-Processed Transparent Conducting Electrodes for Flexible Organic Solar Cells with 16.61% Efficiency. Nano-Micro Letters. 2021;13.
- [19] Grilli M, Di Sarcina I, Bossi S, Rinaldi A, Pilloni L, Piegari A. Ultrathin and stable Nickel films as transparent conductive electrodes. Thin Solid Films. 2015;594:261-5.
- [20] Shtein M. Thin metal films as simple transparent conductors. SPIE Newsroom. 2009;10:1848.
- [21] Song YS, Seong NJ, Choi KJ, Ryu SO. Optical and electrical properties of transparent conducting gallium-doped ZnO electrodes prepared by atomic layer deposition for application in organic solar cells. Thin Solid Films. 2013;546:271-4.
- [22] Basarir F, Irani FS, Kosemen A, Camic BT, Oytun F, Tunaboylu B, et al. Recent progresses on solution-processed silver nanowire based transparent conducting electrodes for organic solar cells. Materials Today Chemistry. 2017;3:60-72.
- [23] Lee J-Y, Connor ST, Cui Y, Peumans P. Solution-Processed Metal Nanowire Mesh Transparent Electrodes. Nano Letters. 2008;8:689-92.
- [24] Fan Q, Zhang Q, Zhou W, Yang F, Zhang N, Xiao S, et al. Highly conductive and transparent carbon nanotube-based electrodes for ultrathin and stretchable organic solar cells. Chinese Physics B. 2017;26:028801.
- [25] Garg R, Elmas S, Nann T, Andersson MR. Deposition methods of graphene as electrode material for organic solar cells. Advanced Energy Materials. 2017;7:1601393.
- [26] Katsnelson MI. Graphene: carbon in two dimensions. Materials Today. 2007;10:20-7.
- [27] Wassei JK, Kaner RB. Graphene, a promising transparent conductor. Materials Today. 2010;13:52-9.
- [28] Emmott CJ, Urbina A, Nelson J. Environmental and economic assessment of ITO-free electrodes for organic solar cells. Solar Energy Materials and Solar Cells. 2012;97:14-21.
- [29] Choi Y-Y, Kang SJ, Kim H-K, Choi WM, Na S-I. Multilayer graphene films as transparent electrodes for organic photovoltaic devices. Solar Energy Materials and Solar Cells. 2012;96:281-5.
- [30] Park H, Chang S, Zhou X, Kong J, Palacios Ts, Gradečak S. Flexible graphene electrode-based organic photovoltaics with record-high efficiency. Nano Letters. 2014;14:5148-54.
- [31] Li Y, Wang B, Hu H, Zhang J, Wei B, Yang L. Pseudo-Biological Highly Performance Transparent Electrodes Based on Capillary Force-Welded Hybrid AgNW Network. IEEE Access. 2019;7:177944-53.

- [32] Wang P, Jian M, Zhang C, Wu M, Ling X, Zhang J, et al. Highly Stable Graphene-Based Flexible Hybrid Transparent Conductive Electrodes for Organic Solar Cells. Advanced Materials Interfaces. 2022;9:2101442.
- [33] Lima L, Matos C, Gonçalves L, Salvatierra R, Cava C, Zarbin A, et al. Water based, solution-processable, transparent and flexible graphene oxide composite as electrodes in organic solar cell application. Journal of Physics D: Applied Physics. 2016;49:105106.
- [34] Ricciardulli AG, Yang S, Feng X, Blom PW. Solution-processable high-quality graphene for organic solar cells. ACS applied materials & interfaces. 2017;9:25412-7.
- [35] Zhang Y, Zhang L, Zhou C. Review of chemical vapor deposition of graphene and related applications. Accounts of chemical research. 2013;46:2329-39.
- [36] Xin H, Li W. A review on high throughput roll-to-roll manufacturing of chemical vapor deposition graphene. Applied Physics Reviews. 2018;5:031105.
- [37] Saeed M, Alshammari Y, Majeed SA, Al-Nasrallah E. Chemical vapour deposition of graphene—Synthesis, characterisation, and applications: A review. Molecules. 2020;25:3856.
- [38] Lin Y-C, Lu C-C, Yeh C-H, Jin C, Suenaga K, Chiu P-W. Graphene annealing: how clean can it be? Nano letters. 2012;12:414-9.
- [39] Lin Y-C, Jin C, Lee J-C, Jen S-F, Suenaga K, Chiu P-W. Clean transfer of graphene for isolation and suspension. ACS nano. 2011;5:2362-8.
- [40] Park H, Brown PR, Bulović V, Kong J. Graphene as transparent conducting electrodes in organic photovoltaics: studies in graphene morphology, hole transporting layers, and counter electrodes. Nano letters. 2012;12:133-40.
- [41] Zhang Z, Du J, Zhang D, Sun H, Yin L, Ma L, et al. Rosin-enabled ultraclean and damage-free transfer of graphene for large-area flexible organic light-emitting diodes. Nature communications. 2017;8:1-9.
- [42] Sun J, Chen Y, Cai X, Ma B, Chen Z, Priydarshi MK, et al. Direct low-temperature synthesis of graphene on various glasses by plasma-enhanced chemical vapor deposition for versatile, cost-effective electrodes. Nano Research. 2015;8:3496-504.
- [43] Tran V-D, Pammi S, Park B-J, Han Y, Jeon C, Yoon S-G. Transfer-free graphene electrodes for super-flexible and semi-transparent perovskite solar cells fabricated under ambient air. Nano Energy. 2019;65:104018.
- [44] Wei N, Li Q, Cong S, Ci H, Song Y, Yang Q, et al. Direct synthesis of flexible graphene glass with macroscopic uniformity enabled by copper-foam-assisted PECVD. Journal of Materials Chemistry A. 2019;7:4813-22.
- [45] Kamel MS, Oelgemöller M, Jacob MV. Sustainable plasma polymer encapsulation materials for organic solar cells. Journal of Materials Chemistry A. 2022.
- [46] Zafar MA, Varghese OK, Robles Hernandez FC, Liu Y, Jacob MV. Single-Step Synthesis of Nitrogen-Doped Graphene Oxide from Aniline at Ambient Conditions. ACS Applied Materials & Interfaces. 2022;14:5797-806.
- [47] Al-Jumaili A, Zafar MA, Bazaka K, Weerasinghe J, Jacob MV. Bactericidal Vertically Aligned Graphene Networks Derived from Renewable Precursor. Carbon Trends. 2022:100157.
- [48] Kumar V, Kumar A, Lee D-J, Park S-S. Estimation of number of graphene layers using different methods: a focused review. Materials. 2021;14:4590.
- [49] Alancherry S, Bazaka K, Levchenko I, Al-Jumaili A, Kandel B, Alex A, et al. Fabrication of nano-onion-structured graphene films from citrus sinensis extract and their wetting and sensing characteristics. ACS Applied Materials & Interfaces. 2020;12:29594-604.
- [50] Kaindl R, Jakopic G, Resel R, Pichler J, Fian A, Fisslthaler E, et al. Synthesis of Graphene-layer Nanosheet Coatings by PECVD. Materials Today: Proceedings. 2015;2:4247-55.
- [51] Ouyang B, Zhang Y, Zhang Z, Fan HJ, Rawat RS. Green synthesis of vertical graphene nanosheets and their application in high-performance supercapacitors. RSC Advances. 2016;6:23968-73.

- [52] Gengenbach TR, Major GH, Linford MR, Easton CD. Practical guides for x-ray photoelectron spectroscopy (XPS): Interpreting the carbon 1s spectrum. Journal of Vacuum Science & Technology A: Vacuum, Surfaces, and Films. 2021;39:013204.
- [53] Blume R, Rosenthal D, Tessonnier JP, Li H, Knop-Gericke A, Schlögl R. Characterizing graphitic carbon with X-ray photoelectron spectroscopy: a step-by-step approach. ChemCatChem. 2015;7:2871-81.
- [54] Morgan DJ. Comments on the XPS Analysis of Carbon Materials. C. 2021;7:51.
- [55] Baer DR, Artyushkova K, Brundle CR, Castle JE, Engelhard MH, Gaskell KJ, et al. Practical guides for x-ray photoelectron spectroscopy: First steps in planning, conducting, and reporting XPS measurements. Journal of Vacuum Science & Technology A. 2019;37.
- [56] Jacob MV, Rawat RS, Ouyang B, Bazaka K, Kumar DS, Taguchi D, et al. Catalyst-Free Plasma Enhanced Growth of Graphene from Sustainable Sources. Nano Letters. 2015;15:5702-8.
- [57] Miccoli I, Edler F, Pfnür H, Tegenkamp C. The 100th anniversary of the four-point probe technique: the role of probe geometries in isotropic and anisotropic systems. Journal of Physics: Condensed Matter. 2015;27:223201.
- [58] Topsoe H. Geometric factors in four point resistivity measurement. Bulletin. 1968;472:63.
- [59] Kholmanov IN, Magnuson CW, Aliev AE, Li H, Zhang B, Suk JW, et al. Improved electrical conductivity of graphene films integrated with metal nanowires. Nano letters. 2012;12:5679-83.
- [60] Zhang F, Zhuo Z, Zhang J, Wang X, Xu X, Wang Z, et al. Influence of PC60BM or PC70BM as electron acceptor on the performance of polymer solar cells. Solar Energy Materials and Solar Cells. 2012;97:71-7.
- [61] Wright M, Uddin A. Organic—inorganic hybrid solar cells: A comparative review. Solar Energy Materials and Solar Cells. 2012;107:87-111.
- [62] He Y, Li Y. Fullerene derivative acceptors for high performance polymer solar cells. Physical Chemistry Chemical Physics. 2011;13:1970-83.
- [63] Noh Y-J, Kim S-S, Kim T-W, Na S-I. Effect of sheet resistance of Ag-nanowire-based electrodes on cell-performances of ITO-free organic solar cells. Semiconductor science and technology. 2013;28:125008.
- [64] Su Y-J, Nie H, Chang C-F, Huang S-C, Huang Y-H, Chen T-W, et al. Green-Solvent-Processable Organic Photovoltaics with High Performances Enabled by Asymmetric Non-Fullerene Acceptors. ACS Applied Materials & Interfaces. 2021;13:59043-50.
- [65] Hosseini SM, Tokmoldin N, Lee YW, Zou Y, Woo HY, Neher D, et al. Putting order into PM6: Y6 solar cells to reduce the Langevin recombination in 400 nm thick junction. Solar RRL. 2020;4:2000498.
- [66] Yuan J, Zhang Y, Zhou L, Zhang G, Yip H-L, Lau T-K, et al. Single-Junction Organic Solar Cell with over 15% Efficiency Using Fused-Ring Acceptor with Electron-Deficient Core. Joule. 2019;3:1140-51.